RSC Advances

PAPER

View Article Online
View Journal | View Issue

Cite this: *RSC Adv.*, 2023, **13**, 14171

Modification of Mg/Al-LDH by vanadate: effects on tribological properties and corrosion resistance

Lixia Ying, Di Wang, Chongyang Nie, * Tianlin Zhu, Fangping Cao, Ruxin Liu and Zhiyong Wang

In this study, Mg/Al layered double hydroxide (LDH) composite coatings were prepared on the surface of anodized 1060 aluminum alloy by an *in situ* growth method, and then the vanadate anions were embedded in the interlayer corridor of LDH by an ion exchange process. The morphology, structure and composition of the composite coatings were investigated using scanning electron microscopy, energy dispersive spectroscopy, X-ray diffractometry and Fourier transform infrared spectroscopy. Ball-and-disk friction wear experiments were carried out to measure the coefficient of friction, the amount of wear, and the morphology of the worn surface. The corrosion resistance of the coating is studied using dynamic potential polarisation (Tafel) and electrochemical impedance spectroscopy (EIS). The results showed that the LDH composite coating with unique layered nanostructure as a solid lubricating film can effectively improve the friction and wear reduction performance of the metal substrate. Chemical modification treatment by embedding vanadate anions in the LDH coating leads to the change of LDH layer spacing and the increase of interlayer channels, resulting in the best friction and wear reduction and corrosion resistance of the LDH coating. Finally, the mechanism of hydrotalcite coating as a solid lubricating film for friction and wear reduction is proposed.

Received 13th March 2023
Accepted 2nd May 2023

DOI: 10.1039/d3ra01636f

rsc.li/rsc-advances

1 Introduction

Aluminum alloys have the advantages of low density, high mechanical strength, good electrical and thermal conductivity, and excellent manufacturability, making them widely used in automotive, aerospace, transportation, and marine applications.[1–3] However, aluminum and its alloys are susceptible to corrosion in aqueous solutions, and their higher coefficient of friction and poor wear resistance limit their large-scale use. In addition, in exposed atmospheric environments, aluminum alloys generate a protective nanoscale film on their surfaces that is highly susceptible to damage,[4] which can lead to the breakdown and corrosion of this film in some extreme environments.[5,6] In order to further expand the application range of aluminum alloys, it is of great practical significance to make aluminum alloys with good friction and wear reduction and corrosion resistance at the same time.

Layered double hydroxides are a class of anionic layered compounds consisting of interlayer anions (An) sandwiched between positively charged (trivalent and divalent cations) laminates with the structural general formula $[M^{2+}_{1-x}M^{3+}_{x}(OH)_2]^{x+}(A^{n-})_{x/n}\cdot yH_2O$, where M^{2+} is a divalent metal cation, M^{3+} is a trivalent metal cation, and A^{n-} is the interlayer anion.[7,8] Due to its unique laminar structure, the versatility of the combination of laminate cations and interlayer anions makes LDH highly attractive in practical applications. Currently, LDH has been widely used in metal corrosion protection,[9–11] frictional wear,[12,13] *etc.*

The potential applications of LDH for the protection of metals and alloys have been extensively investigated and hydrotalcite films have been successfully prepared on metal and alloy substrates. For example, Wu *et al.*[14–17] synthesized a series of superhydrophobic and corrosion-resistant hydrotalcite films on magnesium alloys and investigated the *in situ* growth behavior of hydrotalcite films, proposing a SK growth model from two-dimensional growth (2D) to three-dimensional growth (3D) to explain the transition process from anodic to hydrotalcite films. Chen *et al.*[18,19] used a two-step method to grow Mg–Al hydrotalcite films *in situ* on magnesium alloys, first forming a precursor film with a reticulated crack structure and then transforming the film into a dense and homogeneous hydrotalcite film in a post-treatment. Iqbal M. A. *et al.*[20–24] prepared various types of hydrotalcite films on aluminum alloys and investigated the effect of synthesis conditions on the geometry, growth rate, and corrosion resistance of hydrotalcite films. Recently, more researchers have shown great interest in growing hydrotalcite films on anodic films rather than directly on bare metal substrates.[25–29]

LDH can achieve a variety of special functions due to its interlayer anion replaceable property. The intercalation of some organic anions increases the height of the interlayer channels of

College of Mechanical and Electrical Engineering, Harbin Engineering University, Harbin, 150001, China

LDH, which gives the upper and lower laminates a larger relative slip space and plays a good role in friction reduction.[30,31] The LDH is modified by introducing ions with corrosion inhibitor function to improve its corrosion resistance,[32–36] in which the blocking of corrosive substances and the release of corrosion inhibitor will delay the process of coating failure, and the degree of coating protection varies according to the corrosion inhibitor anion, and among many corrosion inhibitors, vanadate has an excellent corrosion inhibition effect. In a corrosive environment, LDH loaded with vanadate plays the dual role of capturing corrosive chloride ions to reduce the chloride ion concentration and releasing the anionic corrosion inhibitor to the metal surface and adequately protecting the surface.[11] LDH films double-doped with rare earth elements cerium and vanadate can maintain good stability in NaCl solutions, mainly attributed to the synergistic effect of cerium ions and vanadate anions.[37] Vanadate has been widely used as a corrosion inhibitor to modify LDH coatings, however, the tribological properties of vanadate intercalated LDH have not been reported, especially the dual effect of vanadate on the tribological properties and corrosion resistance of LDH composite coatings.

In this work, LDH composite film layers loaded with vanadate ions were prepared on anodized aluminum alloys by a simple two-step process, aiming to investigate the effects of vanadate ions on the corrosion resistance and tribological properties of LDH composite film layers. The morphology and microstructure of the composite film layers were studied by scanning electron microscopy (SEM), Fourier transform infrared spectroscopy (FT-IR) and X-ray diffraction (XRD). The corrosion behavior in 3.5% NaCl solution was investigated using kinetic potential and electrochemical impedance spectroscopy (EIS). Tribological tests were carried out using a ball-and-disk friction tester, and the wear mechanism of the LDH composite film layer as a solid lubricating film was proposed based on the analysis of friction coefficient, wear weight loss, and wear surface morphology.

2 Experiment

2.1 Experimental materials and methods

The substrate was 1060 aluminum alloy, and the following chemicals were used in this work: magnesium nitrate hexahydrate ($Mg(NO_3)_2 \cdot 6H_2O$, ≥99.0%), ammonium nitrate (NH_4NO_3, ≥99.0%), ammonia solution ($NH_3 \cdot H_2O$), sodium metavanadate ($NaVO_3$, ≥99.5%), sodium hydroxide (NaOH), and deionized water was used as solvent. Fig. 1 briefly illustrates the process of preparing a layered double hydroxide composite coating on an aluminum alloy substrate. Before anodizing, the substrate is polished with water-resistant sandpaper, ultrasonically cleaned in a mixture of ethanol and acetone for 5 min to remove surface oil, alkaline cleaned in a sodium hydroxide based alkaline cleaning solution and acid cleaned in a 40 g L^{-1} nitric acid solution, and repeatedly cleaned with deionized water at the end of each step. Anodic oxidation is carried out in 0.3 mol L^{-1} phosphoric acid solution, and the outside of the electrolytic cell is cooled by circulating water to maintain the temperature at about 20 °C. The oxidation is carried out at a current density of 0.01 A cm^{-2} for 60 min, and graphite is used as the cathode during the anodic oxidation. After the anodic oxidation process, the specimens were rinsed with deionized water and dried at room temperature. $Mg(NO_3)_2 \cdot 6H_2O$ (2.56 g) and NH_4NO_3 (4.8 g) were dissolved in deionized water (100 ml) and the pH was adjusted to 10 by slowly adding 1% ammonia solution, and the solution was put into an autoclave (100 ml), and the aluminum substrate was immersed vertically in the above solution and reacted hydrothermally at 100 °C for 18 h. After the reaction, the aluminum plate with LDH was removed and rinsed with deionized water and dried at room temperature. The intercalation modification of hydrotalcite was achieved by the anion exchange reaction of hydrotalcite precursors with nitrate structures. An aqueous solution of 0.1 M $NaVO_3$ was prepared, and the pH was adjusted to 8.4 by slowly adding dilute aqueous sodium hydroxide dropwise. Subsequently, the solution was placed in an autoclave, and the aluminum substrate with LDH coating was dipped vertically into the aqueous $NaVO_3$ solution and reacted hydrothermally at 50 °C for 0.5 h, 1 h, 1.5 h and 2 h. Thereafter, the oxidized 1060 aluminum alloy, the LDH before and after vanadate modification is called AAO, LN and LV-0.5, LV-1, LV-1.5, LV-2.

2.2 Testing and characterization methods

In this paper, a Hitachi SU5000 high-tech thermal field type field emission scanning electron microscope was used for electron microscope observation (SEM) and energy dispersive analysis (EDS). The DX-2700B X-ray diffractometer was used to analyze the crystal structure of the sample with a scanning angle of 5°–70°, a speed of 5° min^{-1} and a step width of 0.02°. Spectroscopic analysis was performed using a Spectrum 100 series Fourier transform infrared spectrometer from PerkinElmer, USA, to obtain the functional groups of the samples. Electrochemical tests were used to evaluate the corrosion protection properties of the coatings. The corrosion resistance of the prepared samples was tested using the Shanghai Chenhua CHI760E electrochemical workstation, which included potentiodynamic polarization (Tafel) and electrochemical impedance spectroscopy (EIS) tests. The testing was conducted using a three-electrode two-circuit system, in which samples with different film layers were used as the working electrode, a saturated calomel electrode was used as the reference electrode, and a platinum wire electrode was used as the counter electrode. Due to the presence of a large number of ions and redox substances in seawater, these substances have a significant impact on the corrosion of materials. To simulate the chemical composition of seawater, a 3.5 wt% NaCl solution was used as the corrosion testing solution and tests were conducted at room temperature. The tribological properties of the samples were evaluated by using SFT-2M ball and disc type tribological wear tester with a speed of 200 rpm, a load of 100 g and a time of 30 min. After the friction experiments, the tribological properties of the samples were evaluated by analyzing the friction coefficient, wear volume and abrasion marks.

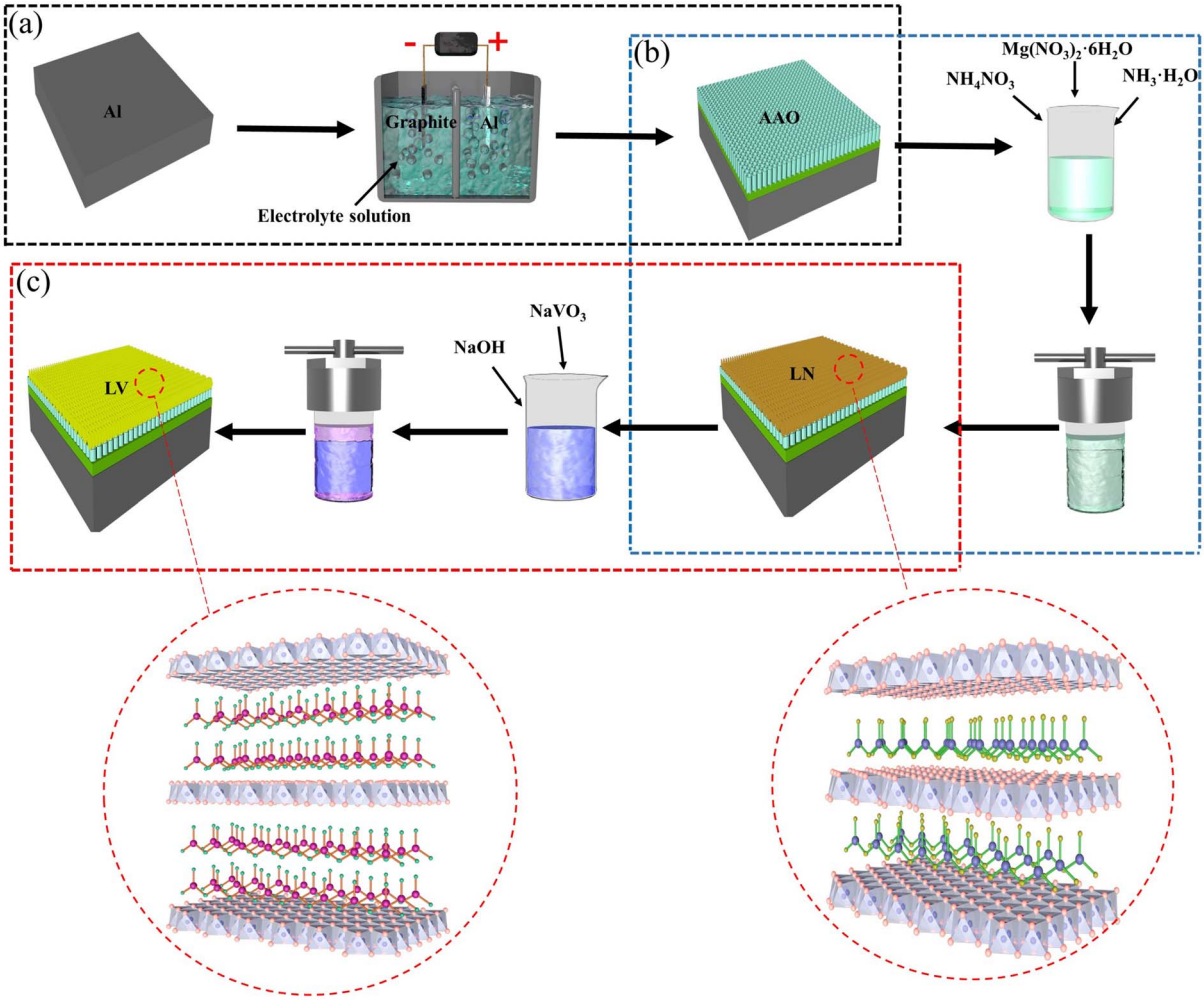

Fig. 1 Schematic diagram of the experimental flow: (a) anodizing of 1060 aluminum alloy, (b) *in situ* synthesis of LN and (c) *in situ* synthesis of LV.

3 Results and discussion

3.1 Surface morphology and EDS analysis

The LDH composite coating is shown in Fig. 2. From Fig. 2a, it is clear that LN nanosheets have a fluffy morphology and dense and uniform growth of hydrotalcite microcrystals on the surface. Compared with LN, the vanadate intercalation changed the surface morphology of LDH. the reaction time was 0.5 h, the basic morphology of LDH nanosheets did not change significantly, and they still showed a fluffy shape, but the overall size

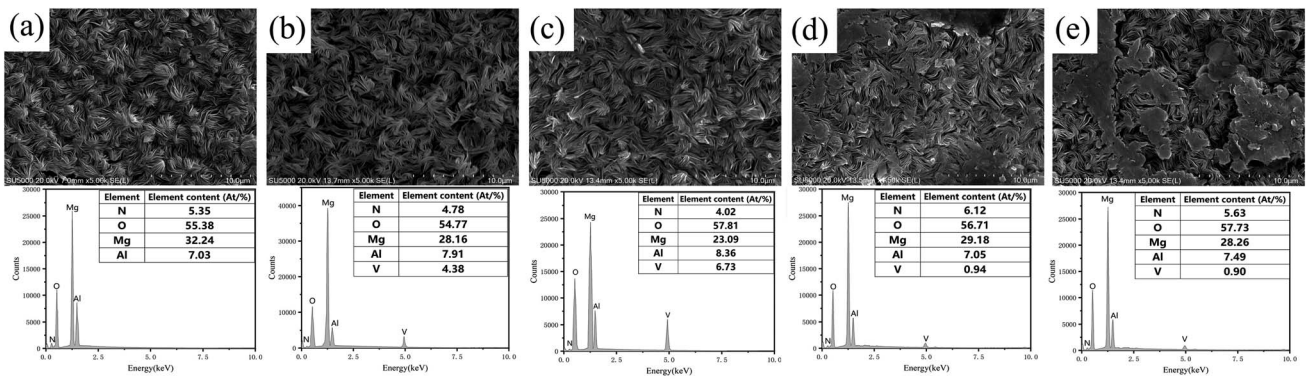

Fig. 2 SEM images and EDS data of LN composite coating (a) and LV composite coating at different reaction times: 0.5 h (b), 1 h (c), 1.5 h (d), 2 h (e).

of LDH nanosheets decreased and the surface morphology was sparse, and when the reaction time was 1 h, the shape of LDH nanosheets stretched from the cluster fluffy shape of the precursor to a slender hair-like shape, and the decrease in size was attributed to the fragmentation caused by the rapid exchange of initial ions, and the surface of the film became more dense. This can be attributed to the increase in substrate spacing due to vanadate intercalation; when the reaction time continued to increase, the hydrotalcite film morphology changed considerably, and it was no longer the fluffy shape of the precursor but the hydrotalcite nanoflakes stacked together in a scale-like covering on the surface.

As seen from the EDS, LN was found to contain mainly elemental magnesium, aluminum, nitrogen and oxygen, which proves the successful synthesis of LDH using alumina as a cation source. In the EDS analysis of the hydrotalcite films modified with vanadate, elemental vanadium appeared after the ion exchange process, a result that proves the successful intercalation of vanadate anions into the interlayer channels of LDH.

3.2 Chemical and phase composition

Fig. 3a shows the XRD spectra of LN and LV composite coatings synthesized by the *in situ* growth method, and it can be observed from Fig. 1 that the characteristic diffraction peaks of LDH on the crystalline planes of (003), (006), (012), and (110) appear around $2\theta = 9.98°$, 20.18°, 34.34°, and 59.82°, respectively, and no other spurious peaks appear, and the crystalline. The diffraction peaks are narrow and sharp in shape with smooth baselines, indicating the synthesis of LN with good crystallinity, which is consistent with the results of previous studies.[38] It is worth noting that after the exchange with vanadate anion, the characteristic diffraction peaks appearing on (003) and (006) crystal faces move forward, thus proving that VO_3^- enters between the lamellae.[39,40]

The interlaminar distances were calculated according to the Bragg equation ($2d \sin\theta = n\lambda$) and the corresponding interlaminar channel heights were obtained after deducting the laminate thickness of 0.48 nm[41] and the results are shown in Table 1.

As shown in Table 1, the interlayer channel heights of LV were all increased after the ion exchange reaction compared to LN. From the figure and table, we can see that the LV (003) synthesized under the condition of $t = 1$ h has the highest crystalline diffraction intensity and the largest distance shifted to a small angle, indicating that the LDH synthesized under this condition has the best crystallinity and the highest interlayer channel height.

Fig. 3b shows the FTIR spectra of LN and vanadate-loaded LV. For LN, the peaks located at 3750, 3500, and 1640 cm^{-1} correspond to symmetric contraction and bending vibrations of H–O–H, O–H, and water molecules attributed to the presence of surface absorbed water and interlayer water, the peak located at 1387 cm^{-1} is designated as the ν_3 stretching vibration of the NO-3 group in the hydrotalcite intercalation, and the other bands observed at 500–800 are due to M–O, M–O–M, and O–M–O lattice vibrations, with additional bands observed at 2408 cm^{-1}, which can be attributed to adsorbed CO_2.[42] After the anion exchange, a new absorption peak appears at 940 cm^{-1} due to VO-3 stretching vibrations, indicating the presence of VO-3 in the intercalation. In addition, it is noteworthy that the absorption peak of NO-3 is still observed, indicating that nitrate is not completely replaced by vanadate.[43] Based on the above FTIR spectral analysis, combined with the above microscopic characterization method, we can conclude that VO-3 ions are

Table 1 XRD data of LN composite coating and LV composite coating synthesized under different reaction times

Sample	Reaction time (h)	2θ (°)	Interlayer distance (003)/nm	Gallery height (nm)
LN	—	9.98	0.88	0.40
LV-0.5	0.5	9.42	0.94	0.46
LV-1	1	9.34	0.95	0.47
LV-1.5	1.5	9.4	0.94	0.46
LV-2	2	9.44	0.93	0.45

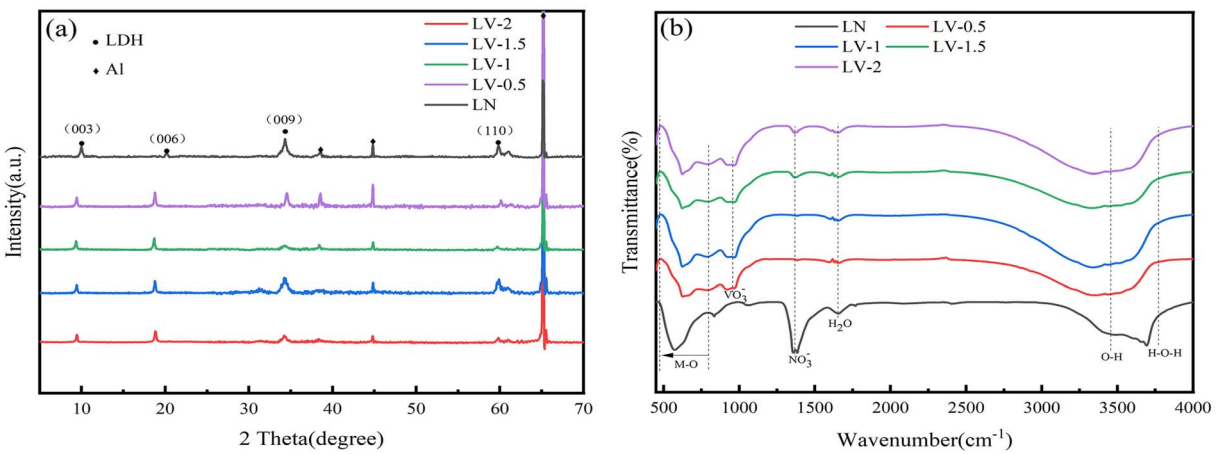

Fig. 3 XRD spectra (a) and FTIR spectra (b) of LDH-NO-3 and LDH-VO-3 composite coatings with different reaction times.

successfully intercalated into the interlayer channels of LDHs through an anion exchange process.

3.3 Corrosion resistance

The dynamic potential polarization curves of LDH coating and alumina substrate in 3.5 wt% solution are given in Fig. 4, and the corrosion potential (E_{corr}) and corrosion current density (i_{corr}) are shown by the polarization test results in Table 2. The corrosion potential mainly describes the corrosion tendency of the sample, while the dynamic corrosion is described by the corrosion current density, and the smaller the corrosion current density value of the sample the higher its dynamic corrosion resistance.[27] From Table 2, we can know that AAO has the lowest corrosion potential (−0.85 V) and the highest corrosion current density (2.159×10^{-7} A cm^{-2}) among all samples, which may be due to the presence of pores on the surface of AAO, thus leading to its low corrosion resistance. In addition, we can see that the substrate with LN and LV composite coatings has one and two orders of magnitude lower corrosion current density compared to the AAO substrate, which is due to the fact that LDH nanosheets seal the surface pores of AAO and protect the substrate, while the LV composite coating has superior corrosion resistance due to the vanadate anion on the one hand can trap corrosive chloride ions on the one hand, and release retardants to protect the substrate surface on the other. Importantly, all LDH coatings protect the AAO substrate, and LV-1 has the highest corrosion potential (−0.42 V) and the lowest corrosion current density (3.421×10^{-9} A cm^{-2}) among all samples, indicating the best corrosion resistance.

To further provide a characterization of the corrosion inhibition effect of the LDH composite coating, an electrochemical impedance spectroscopy (EIS) analysis of the corrosion resistance of the coating was performed. The corresponding fitting circuit was depicted in Fig. 5a. In the figure, (1) represents the equivalent circuit model of the alumina substrate, where R_s is the solution resistance, R_{fp} is the resistance of the substrate surface film, CPE_{fp} is the capacitance at the substrate and interface, R_{ct} is the charge transfer resistance, and C_{dl} is the corresponding capacitance. (2) Represents the equivalent circuit model of LDH and composite-modified LDH, where R_s is the solution resistance, R_{fp} is the outer resistance of the coating, CPE_{fp} is the capacitance at the film and solution interface, R_{fd} is the inner resistance of the film, CPE_{fd} is the inner capacitance of the film, R_{ct} is the charge transfer resistance, and C_{dl} is the double-layer capacitance outside the interface.

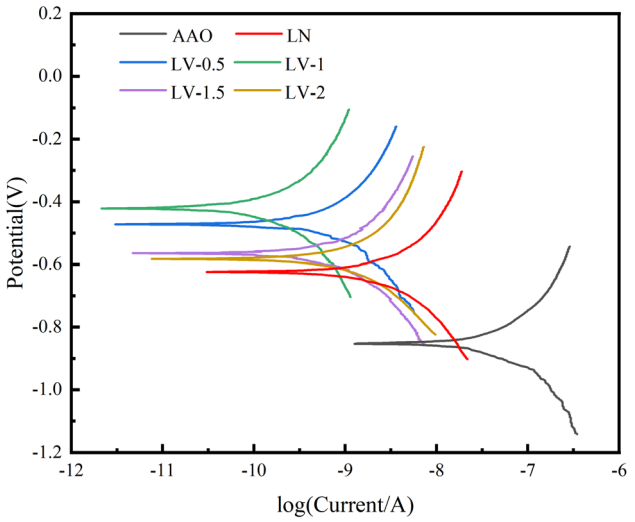

Fig. 4 Dynamic potential polarization curves of AAO substrate with LDH composite coating.

Fig. 5b is a typical Bode plot, and it is well known that a higher low frequency impedance modulus (Z) at a lower frequency represents better corrosion resistance, and it can be seen from the Bode plot that LV-1 exhibits the maximum impedance at low frequencies. Meanwhile, Fig. 5c shows a typical Nyquist plot, from which it can be observed that the LV-1 coating has the largest radius of curvature indicating that this sample has the highest corrosion resistance. The LV-1 composite coating has the highest low-frequency impedance modulus (Z) and the largest radius of curvature compared with other coating samples, indicating that the composite coating under this condition has the best corrosion resistance and can effectively prevent the diffusion of chloride ions into the aluminum alloy substrate, thus reducing the corrosion rate of the aluminum alloy substrate. The results are consistent with the dynamic potential polarization curves (Table 3).

3.4 Tribological performance analysis

As shown in Table 4, the LN composite coating has a good friction reduction effect, in which the LV composite coating with vanadate loading achieves a further reduction in the friction coefficient. The coefficient of friction curve of AAO and LDH composite coating is shown in Fig. 6a. The coefficient of friction curve of AAO stabilized at about 0.85 after a short rise. At the beginning of the friction test, the relative motion of the AAO substrate and the friction substrate occurred, resulting in the generation of grooves and debris, larger surface roughness values on the couple surfaces, smaller actual contact areas, and severe adhesion at the contact points, this stage is called the running-in wear stage, and the friction coefficient gradually increased. As the test continues, the wear surface gradually stabilizes and the friction coefficient remains at a stable value. This stage is called the stable wear stage, where the wear is slow and stable and the friction coefficient remains basically unchanged. The friction coefficient curve of the sample with LN coating showed a relatively stable friction coefficient curve, which was attributed to the strong adhesion between LDH nanosheets and AAO, the dense and smooth surface of the coating, and the uniform distribution of LDH nanosheets, which did not cause the LDH coating to break at the beginning of the test, and as the test proceeded, the LDH coating began to break, and the resulting debris adhered to the surface of the friction pair while being fed back to the coating, and the friction coefficient continued to remain stable without large fluctuations. The friction coefficient of the LV composite coating loaded with vanadate at different reaction times shows that the

Table 2 Dynamic potential polarization parameters of AAO substrate and LDH composite coating

Sample	E_{corr} (V/SCE)	i_{corr} (A cm^{-2})	β_a (mV dec^{-1})	$-\beta_c$ (mV dec^{-1})	R_p (Ω cm^2)
AAO	−0.85	2.159×10^{-7}	76.53	100.32	8.73×10^{4}
LN	−0.62	3.652×10^{-8}	153.82	242.54	1.12×10^{6}
LV-0.5	−0.47	3.874×10^{-9}	526.71	353.52	2.42×10^{7}
LV-1	−0.42	3.421×10^{-9}	622.46	367.36	2.93×10^{7}
LV-1.5	−0.56	5.309×10^{-9}	377.34	252.67	1.23×10^{7}
LV-2	−0.58	5.421×10^{-9}	327.48	267.29	1.18×10^{7}

friction coefficient drops sharply at the initial stage of wear, and then enters a stable wear stage where the friction coefficient remains at a relatively stable value. This is due to the ion exchange reaction process that makes the LV composite coating become loose and rough. At the beginning of the test, the roughness is large and the friction coefficient is large. As the test proceeds, the friction sub and the composite coating gradually wear together, the surface of the coating gradually becomes smooth and the friction coefficient starts to drop sharply and remains stable. The friction coefficients of LV composite coating loaded with vanadate at different reaction times and LN composite coating showed large differences in wear characteristics and values, among which LV-1 friction coefficient was the lowest, indicating that the composite coating prepared at this reaction time had the most excellent tribological properties.

Fig. 6b shows the wear weight loss of AAO and LDH composite film layer under dry friction conditions. As shown in the figure, AAO has the largest wear loss during the dry friction test, which corresponds to the SEM photograph in Fig. 7a, the AAO wear marks have a rough surface with more grooves, and the peeling of the matrix surface layer makes the AAO lose the most weight. The LV-1 composite coating has the lowest wear weight loss, much less than that of the AAO matrix, which indicates that the vanadate-loaded composite coating prepared at a reaction time of 1 h has the best tribological properties. LN composite coating has lower wear loss, however, compared with LV, its wear loss is still slightly higher than LV composite coating due to larger friction coefficient.

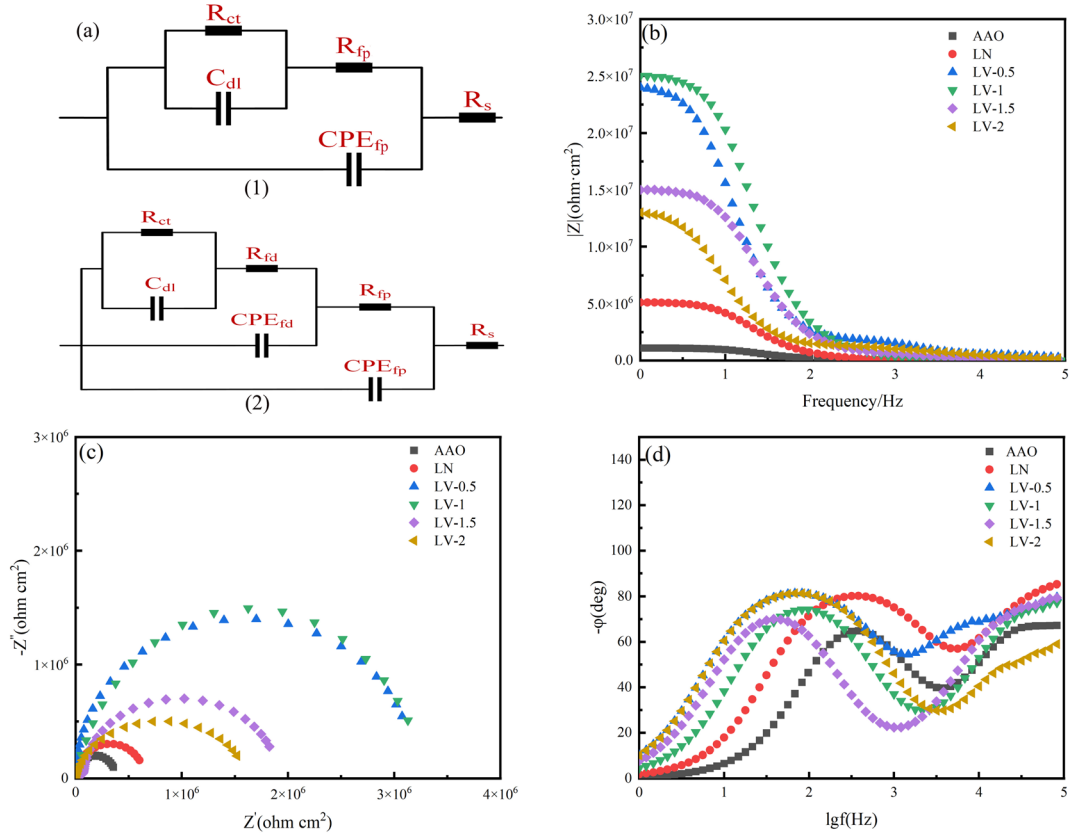

Fig. 5 Equivalent circuits used to fit the EIS spectra of AAO substrate with LDH composite coating (a) potentiodynamic polarization curve: (b) Bode plot, (c) Nyquist plot and (d) phase angle plot.

Table 3 The fitted parameters of EIS spectrum

Sample	R_s (Ω cm^2)	CPE_{fp} (μF cm^{-2})	R_{fp} (Ω cm^2)	CPE_{fd} (μF cm^{-2})	R_{fd} (Ω cm^2)	C_{dl} (μF cm^{-2})	R_{ct} (Ω cm^2)
AAO	11.382	8.375×10^{-8}	1.263×10^{3}	—	—	7.068×10^{-8}	1.109×10^{6}
LN	8.296	2.356×10^{-8}	3.531×10^{3}	6.226×10^{-8}	2.576×10^{3}	2.942×10^{-8}	4.662×10^{6}
LV-0.5	6.921	1.239×10^{-8}	7.207×10^{3}	1.254×10^{-8}	1.027×10^{3}	1.006×10^{-8}	8.429×10^{6}
LV-1	6.872	1.031×10^{-8}	7.656×10^{3}	1.387×10^{-7}	9.635×10^{2}	1.027×10^{-8}	8.531×10^{6}
LV-1.5	7.982	2.132×10^{-8}	3.646×10^{3}	6.897×10^{-8}	2.162×10^{3}	2.683×10^{-8}	4.926×10^{6}
LV-2	8.062	2.148×10^{-8}	3.703×10^{3}	6.821×10^{-8}	2.187×10^{3}	2.733×10^{-8}	4.903×10^{6}

Table 4 Coefficient of friction between AAO matrix and LDH composite coating

Sample	Friction coefficient	Reduction compared with aluminium oxide/%
AAO	0.85	—
LN	0.35	59%
LV-0.5	0.18	79%
LV-1	0.10	88%
LV-1.5	0.18	79%
LV-2	0.21	75%

From the calculation results in Table 1, we can see that the interlayer channel height of LN composite coating used in tribological experiments is 0.40 nm, while the interlayer channel height of LV composite coating loaded with vanadate are improved, and its LV-1 composite coating with a reaction time of 1 h has the highest interlayer channel height of 0.47 nm. Fig. 1 shows the two possible. The reason why the friction reduction effect of LV composite coating is better than that of LN composite coating is that it has a higher interlayer channel height, which makes the upper and lower laminates of hydrotalcite have a larger sliding space and facilitates the relative sliding of the laminates. In the LDH structure, there is a strong electrostatic attraction between the positively charged hydromagnesite-like laminates and the interlayer anions, while the vanadate anion enters the interlayer, which greatly increases the interlayer distance of LDH and thus weakens the electrostatic attractive effect. As a result, with the increase of the interlayer distance, the electrostatic attraction weakens, and the LV low-intensity adjacent laminates are subjected to less resistance during friction and slide more easily relative to each other compared to LN.

The wear scar morphology and EDS analysis results of alumina and its composite film layer are shown in Fig. 7. As shown in Fig. 7a, the alumina substrate has the largest abrasion width, and the microscopic morphology of the abrasion surface is rougher with more abrasion streaks and debris, which indicates that abrasive wear is occurring on the alumina substrate, which in turn is causing the surface layer of the alumina substrate to peel off. Fig. 7b shows the surface microstructure of the LN composite film layer, the width of the abrasion marks in Fig. 7b is significantly smaller than that of the alumina matrix and the coating surface shows larger fragmentation and splitting, which is due to the fracture caused by the steel ball sliding on the coating surface, and the EDS results show that the elemental content of Al is more at this time, but there is still the presence of Mg, which proves that the frictional wear occurs at the junction of the alumina substrate and the LDH film layer. Fig. 7d shows the microscopic shape of the wear surface of LV-1 composite film layer, compared with Fig. 7a and b, the wear surface of this coating is relatively flat, without obvious fragmentation and debris, which indicates that this coating is softer than the alumina matrix, and the coating surface is more uniform, and as the wear proceeds, this coating can compensate for the craters and defects caused by the wear, as shown in the

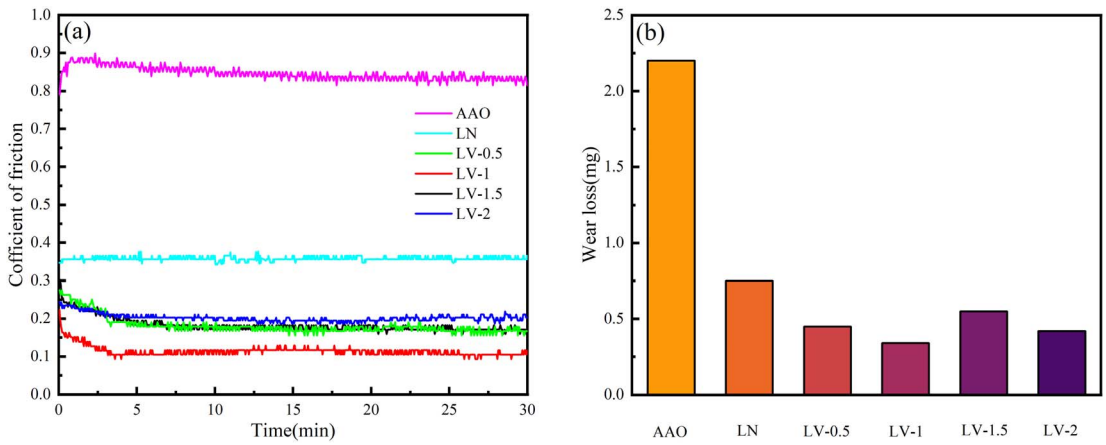

Fig. 6 Friction coefficient curve of AAO and LDH composite coating (a) and abrasion loss weight (b).

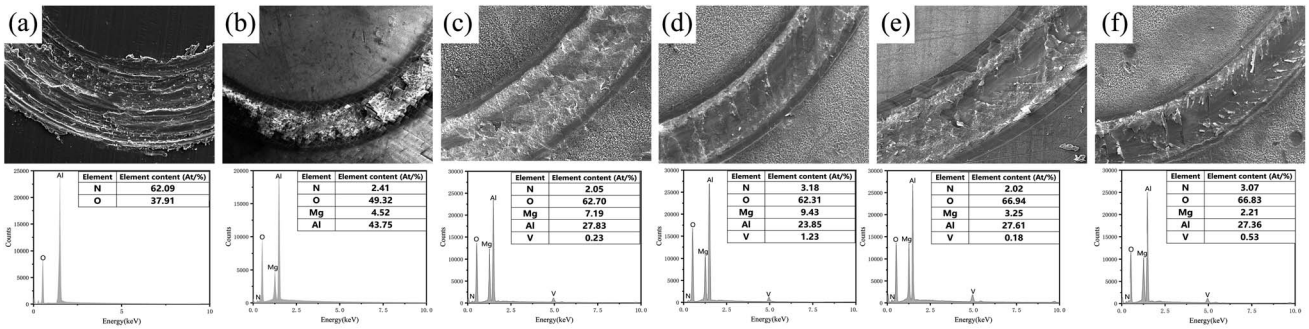

Fig. 7 Surface morphology of wear marks and EDS data of AAO (a), LN composite coating (b) and LV composite coating at different reaction times: 0.5 h (c), 1 h (d), 1.5 h (e), 2 h (f).

EDS analysis results, at this time the oxygen elements and aluminum elements are 62.31% and 23.85%, and a small amount of vanadium elements are found, which indicates that during the process of wear, the steel ball does not completely penetrate the coating, but the steel ball interacts with the coating, and the coating interacts with the substrate and fuses with each other in a process.

The reason why LDH reduces the coefficient of friction is that during the wear process, LDH nanosheets rub against the alumina substrate, generating squeezing pressure and high temperature, and then the deformed LDH nanosheets combine with wear debris to form a lubrication layer between the contact areas, and as the LDHs nanosheets stored in cracks and pores move to the surface as a complement, a continuous process of disappearance and reconstruction of the lubricant layer is produced in the friction wear test. Thus, LDH nanosheets as a solid lubricant are applied to the surface to form a lubricating layer, and the synergistic effect of the wear-resistant coating and the nanosheets improves the wear resistance of the substrate.

4 Conclusion

In this paper, an anodic oxide layer was prepared on 1060 aluminum alloy by anodic oxidation method, and then LN composite coating was grown on this coating by *in situ* growth method, and subsequently the vanadate ion was introduced by using the ion exchangeability between LDH layers, and LV composite coating was prepared at different reaction times (0.5 h, 1 h, 1.5 h, 2 h), and the corrosion resistance and tribological properties of LN and LV composite coatings were tested and analyzed, and the effects of vanadate and reaction time on the corrosion resistance and tribological properties of LV composite coatings were discussed, and the main conclusions were as follows.

(1) The prepared LN composite coatings were dense and homogeneous, and the LDH nanosheets were in a unique fluffy shape, and the size of LV nanosheets decreased while the coating surface became more dense after the exchange with vanadate ions.

(2) All the LDH composite coatings improve the corrosion resistance and tribological properties of AAO substrate to different degrees, and the LV-1 composite coating with 1 h reaction time has the best corrosion resistance, friction reduction and wear resistance, which has the best protection effect on the aluminum alloy substrate.

(3) LDH as a solid lubricating film to improve the friction and wear reduction performance of AAO matrix is attributed to two aspects, on the one hand, the synergistic action of LDH nanosheets and alumina matrix to build a lubricating layer, which is continuously disappearing and reconstructing during the wear process; on the other hand, LV composite coating has higher interlayer channel height, which will make the electrostatic attraction weaken, and the upper and lower laminates have a larger sliding space, which is conducive to the relative sliding of the laminates and reduces the relative sliding resistance.

Conflicts of interest

There are no conflicts to declare.

Acknowledgements

The research was supported by the National Natural Science Foundation of China (No. 52075112), the National Key R & D Program of China for Young Scientists (No. 2021YFB200007), and the Heilongjiang Provincial Natural Science Foundation (No. LH2021E033).

References

1 G. M. Karthik and H. S. Kim, Heterogeneous Aspects of Additive Manufactured Metallic Parts: A Review, *Met. Mater. Int.*, 2021, **27**, 1–39.
2 Q. Z. Chen, Z. Q. Jiang, S. G. Tang, W. B. Dong, Q. Tong and W. Z. Li, Influence of graphene particles on the micro-arc oxidation behaviors of 6063 aluminum alloy and the coating properties, *Appl. Surf. Sci.*, 2017, **423**, 939–950.
3 Y. C. Dun, X. H. Zhao, Y. M. Tang, S. Dino and Y. Zuo, Microstructure and corrosion resistance of a fluorosilane modified silane-graphene film on 2024 aluminum alloy, *Appl. Surf. Sci.*, 2018, **437**, 152–160.

4 S. M. Li, W. H. Yao, J. H. Liu, M. Yu and K. Ma, Effect of SiC nanoparticle concentration on the properties of oxide films formed on Ti-10V-2Fe-3Al alloy, *Vacuum*, 2016, **123**, 1–7.
5 J. Soltis, Passivity breakdown, pit initiation and propagation of pits in metallic materials – review, *Corros. Sci.*, 2015, **90**, 5–22.
6 J. H. Liu, Q. Yu, M. Yu, S. M. Li, K. Zhao, B. Xue and H. Zu, Silane modification of titanium dioxide-decorated graphene oxide nanocomposite for enhancing anticorrosion performance of epoxy coatings on AA-2024, *J. Alloys Compd.*, 2018, **744**, 728–739.
7 J. F. Yu, Q. Wang, D. O'Hare and L. Y. Sun, Preparation of two dimensional layered double hydroxide nanosheets and their applications, *Chem. Soc. Rev.*, 2017, **46**, 5950–5974.
8 Q. Wang and D. O'Hare, Recent Advances in the Synthesis and Application of Layered Double Hydroxide (LDH) Nanosheets, *Chem. Rev.*, 2012, **112**, 4124–4155.
9 X. Wang, C. Jing, Y. X. Chen, X. S. Wang, G. Zhao, X. Zhang, L. Wu, X. Y. Liu, B. Q. Dong and Y. X. Zhang, Active corrosion protection of super-hydrophobic corrosion inhibitor intercalated Mg-Al layered double hydroxide coating on AZ31 magnesium alloy, *J. Magnesium Alloys*, 2020, **8**, 291–300.
10 Q. Q. He, M. J. Zhou and J. M. Hu, Electrodeposited Zn-Al layered double hydroxide films for corrosion protection of aluminum alloys, *Electrochim. Acta*, 2020, **355**, DOI: **10.1016/j.electacta.2020.136796**.
11 J. K. Pancrecious, S. V. Vineetha, U. S. Bill, E. B. Gowd and T. P. D. Rajan, Ni-Al polyvanadate layered double hydroxide with nanoceria decoration for enhanced corrosion protection of aluminium alloy, *Appl. Clay Sci.*, 2021, **211**, DOI: **10.1016/j.clay.2021.106199**.
12 Z. M. Bai, Z. Y. Wang, T. G. Zhang, F. Fu and N. Yang, Characterization and friction performances of Co-Al-layered double-metal hydroxides synthesized in the presence of dodecylsulfate, *Appl. Clay Sci.*, 2013, **75–76**, 22–27.
13 Z. M. Bai, G. J. Li, F. Y. Zhao and H. L. Yu, Tribological Performance and Application of Antigorite as Lubrication Materials, *Lubricants*, 2020, **8**, DOI: **10.3390/lubricants8100093**.
14 L. Wu, G. Zhang, A. T. Tang, Y. L. Liu, A. Atrens and F. S. Pan, Communication-Fabrication of Protective Layered Double Hydroxide Films by Conversion of Anodic Films on Magnesium Alloy, *J. Electrochem. Soc.*, 2017, **164**, C339–C341.
15 L. Wu, D. N. Yang, G. Zhang, Z. Zhang, S. Zhang, A. T. Tang and F. S. Pan, Fabrication and characterization of Mg-M layered double hydroxide films on anodized magnesium alloy AZ31, *Appl. Surf. Sci.*, 2018, **431**, 177–186.
16 G. Zhang, L. Wu, A. T. Tang, X. B. Chen, Y. L. Ma, Y. Long, P. Peng, X. X. Ding, H. L. Pan and F. S. Pan, Growth behavior of MgAl-layered double hydroxide films by conversion of anodic films on magnesium alloy AZ31 and their corrosion protection, *Appl. Surf. Sci.*, 2018, **456**, 419–429.
17 L. Wu, F. S. Pan, Y. H. Liu, G. Zhang, A. T. Tang and A. Atrens, Influence of pH on the growth behaviour of Mg-Al LDH films, *Surf. Eng.*, 2018, **34**, 674–681.
18 J. Chen, Y. W. Song, D. Y. Shan and E. H. Han, In situ growth of Mg-Al hydrotalcite conversion film on AZ31 magnesium alloy, *Corros. Sci.*, 2011, **53**, 3281–3288.
19 J. Chen, Y. W. Song, D. Y. Shan and E. H. Han, Study of the in situ growth mechanism of Mg-Al hydrotalcite conversion film on AZ31 magnesium alloy, *Corros. Sci.*, 2012, **63**, 148–158.
20 M. A. Iqbal, L. Y. Sun, H. Asghar and M. Fedel, Chlorides Entrapment Capability of Various In-Situ Grown NiAl-LDHs: Structural and Corrosion Resistance Properties, *Coatings*, 2020, **10**.
21 M. A. Iqbal and M. Fedel, Effect of operating parameters on the structural growth of ZnAl layered double hydroxide on AA6082 and corresponding corrosion resistance properties, *J. Coat. Technol. Res.*, 2019, **16**, 1423–1433.
22 M. A. Iqbal and M. Fedel, Effect of Synthesis Conditions on the Controlled Growth of MgAl-LDH Corrosion Resistance Film: Structure and Corrosion Resistance Properties, *Coatings*, 2019, **9**.
23 M. A. Iqbal and M. Fedel, The effect of the surface morphologies on the corrosion resistance of in situ growth MgAl-LDH based conversion film on AA6082, *Surf. Coat. Technol.*, 2018, **352**, 166–174.
24 M. A. Iqbal and M. Fedel, Ordering and disordering of in situ grown MgAl-layered double hydroxide and its effect on the structural and corrosion resistance properties, *Int. J. Miner. Metall. Mater.*, 2019, **26**, 1570–1577.
25 M. Mohedano, M. Serdechnova, M. Starykevich, S. Karpushenkov, A. C. Bouali, M. G. S. Ferreira and M. L. Zheludkevich, Active protective PEO coatings on AA2024: role of voltage on in-situ LDH growth, *Mater. Des.*, 2017, **120**, 36–46.
26 M. A. Iqbal, H. Asghar and M. Fedel, Double doped cerium-based superhydrophobic layered double hydroxide protective films grown on anodic aluminium surface, *J. Alloys Compd.*, 2020, **844**.
27 L. Liu, L. Wu, X. B. Chen, D. E. Sun, Y. Chen, G. Zhang, X. X. Ding and F. S. Pan, Enhanced protective coatings on Ti-10V-2Fe-3Al alloy through anodizing and post-sealing with layered double hydroxides, *J. mater. sci. technol.*, 2020, **37**, 104–113.
28 F. Chen, P. H. Yu and Y. Zhang, Healing effects of LDHs nanoplatelets on MAO ceramic layer of aluminum alloy, *J. Alloys Compd.*, 2017, **711**, 342–348.
29 M. A. Iqbal and M. Fedel, Protective Cerium-Based Layered Double Hydroxides Thin Films Developed on Anodized AA6082, *Adv. Mater. Sci. Eng.*, 2020, **2020**.
30 S. Li, H. J. Qin, R. F. Zuo and Z. M. Bai, Friction properties of La-doped Mg/Al layered double hydroxide and intercalated product as lubricant additives, *Tribol. Int.*, 2015, **91**, 60–66.
31 D. Zhao, Z. M. Bai and F. Y. Zhao, Preparation of Mg/Al-LDHs intercalated with dodecanoic acid and investigation of its antiwear ability, *Mater. Res. Bull.*, 2012, **47**, 3670–3675.

32 X. Sun, Q. S. Yao, Y. C. Li, F. Zhang, R. C. Zeng, Y. H. Zou and S. Q. Li, Biocorrosion resistance and biocompatibility of Mg-Al layered double hydroxide/poly(L-lactic acid) hybrid coating on magnesium alloy AZ31, *Front. Mater. Sci.*, 2020, **14**, 426–441.

33 W. Wu, X. Sun, C. L. Zhu, F. Zhang, R. C. Zeng, Y. H. Zou and S. Q. Li, Biocorrosion resistance and biocompatibility of Mg-Al layered double hydroxide/poly-L-glutamic acid hybrid coating on magnesium alloy AZ31, *Prog. Org. Coat.*, 2020, **147**.

34 J. Tedim, A. C. Bastos, S. Kallip, M. L. Zheludkevich and M. G. S. Ferreira, Corrosion protection of AA2024-T3 by LDH conversion films. Analysis of SVET results, *Electrochim. Acta*, 2016, **210**, 215–224.

35 Z. M. Qiu, F. Zhang, J. T. Chu, Y. C. Li and L. Song, Corrosion resistance and hydrophobicity of myristic acid modified Mg-Al LDH/Mg(OH)(2) steam coating on magnesium alloy AZ31, *Front. Mater. Sci.*, 2020, **14**, 96–107.

36 Y. H. Cao, D. J. Zheng, J. S. Luo, F. Zhang, C. Wang, S. G. Dong, Y. L. Ma, Z. Y. Liang and C. J. Lin, Enhanced corrosion protection by Al surface immobilization of in-situ grown layered double hydroxide films co-intercalated with inhibitors and low surface energy species, *Corros. Sci.*, 2020, **164**.

37 Y. Zhang, Y. D. Li, Y. S. Ren, H. Wang and F. Chen, Double-doped LDH films on aluminum alloys for active protection, *Mater. Lett.*, 2017, **192**, 33–35.

38 M. Serdechnova, A. N. Salak, F. S. Barbosa, D. E. L. Vieira, J. Tedim, M. L. Zheludkevich and M. G. S. Ferreira, Interlayer intercalation and arrangement of 2-mercaptobenzothiazolate and 1,2,3-benzotriazolate anions in layered double hydroxides: in situ X-ray diffraction study, *J. Solid State Chem.*, 2016, **233**, 158–165.

39 J. Qu, Q. W. Zhang, X. W. Li, X. M. He and S. X. Song, Mechanochemical approaches to synthesize layered double hydroxides: a review, *Appl. Clay Sci.*, 2016, **119**, 185–192.

40 J. Tedim, M. L. Zheludkevich, A. N. Salak, A. Lisenkov and M. G. S. Ferreira, Nanostructured LDH-container layer with active protection functionality, *J. Mater. Chem.*, 2011, **21**, 15464–15470.

41 G. W. Brindley and C.-C. Kao, Structural and IR relations among brucite-like divalent metal hydroxides, *Phys. Chem. Miner.*, 1984, **10**, 187–191.

42 Z. M. Ni, S. J. Xia, C. P. Fang, L. G. Wang and J. Hu, Synthesis, characterization and thermal property of Cu/Co/Mg/Al hydrotalcite like compounds, *Rare Met. Mater. Eng.*, 2008, **37**, 634–637.

43 G. Zhang, L. Wu, A. T. Tang, S. Zhang, B. Yuan, Z. C. Zheng and F. S. Pan, A Novel Approach to Fabricate Protective Layered Double Hydroxide Films on the Surface of Anodized Mg-Al Alloy, *Adv. Mater. Interfaces*, 2017, **4**.